JOURNAL OF MATERIALS SCIENCE 25 (1990) 3615-3633

Interaction of 18Cr–10Ni stainless steel with liquid aluminium

V. I. DYBKOV
Institut Problem Materialoznavstva, Kiev 252 180, USSR

The dissolution of an 18Cr–10Ni stainless steel in liquid aluminium at 700 to 850° C was found by the rotating disc technique to be non-selective and diffusion controlled. Experimentally determined values of the parameters characterizing the dissolution run are presented. In the case of saturated aluminium melts two intermetallic layers were found to form between the steel and the melt material at 700° C. The compact layer adjacent to the steel surface is probably a solid solution based upon the Fe_2Al_5 compound. Its thickness, x, tends with increasing time to the limiting value $x_{max} = 10\,\mu m$. The porous layer adjacent to the melt material is probably a solid solution based upon the $FeAl_3$ compound. After a certain period of non-linear growth its thickness, y, increases with time, t, according to the linear law: $y = 1 \times 10^{-8} t + 6 \times 10^{-6}$ m. The time dependence of the total thickness of both layers is well described in terms of the "paralinear" kinetics. In the case of undersaturated aluminium melts the formation of a single-phase intermetallic layer, 3 to 11 μm thick, was observed at 700° C for 100 to 600 sec. The steel-to-aluminium transition joints with good mechanical properties were made by interaction of a solid steel material with liquid aluminium.

1. Introduction

If the surface of stainless steel is exposed to liquid aluminium attack, dissolution of steel into aluminium and the growth of the intermetallic layers at the steel–aluminium interface take place. Because an 18Cr–10Ni stainless steel is a complex material containing at least three main constituents (iron, chromium and nickel) there are two possible ways of its dissolution.

The first is a selective dissolution. Such behaviour may be expected in view of significant differences in the solubilities of iron, chromium and nickel in liquid aluminium in the Al–Fe, Al–Cr and Al–Ni binary systems, respectively. Indeed, according to the data of Yeremenko *et al.* [1, 2] the solubility of iron in liquid aluminium in the Al–Fe binary system, say, at 700° C is 2.5 ± 0.1%. (All values of concentration or content are given in mass %. The most important values are followed by their 0.95 confidence limits.) For chromium and nickel the solubilities in binary systems at that temperature are 0.72 ± 0.02% and 10.0 ± 0.5%, respectively. Therefore, enhanced dissolution of nickel from the steel into the aluminium melt compared to that of iron and chromium might be expected. If so, a lowering of the nickel content in the steel bulk would clearly be observed.

The second is a non-selective (uniform) dissolution. An 18Cr–10Ni stainless steel has a single-phase austenitic structure [3]. In its lattice the iron, chromium and nickel atoms are connected together by metallic bonds of nearly equal strength because those elements are the neighbours in the Periodic Table. Therefore, it may be supposed that the iron and chromium atoms, being the major constituents of the steel, will not "permit" the nickel atoms to leave its lattice at a rate which exceeds their own rates of transition into liquid aluminium. From this view-point all the elements should pass into the melt in those ratios in which they are present in the steel.

Thus, it is difficult to decide theoretically which of the two ways of dissolution is preferable. When studying the dissolution of stainless steel and other ferrous alloys in the molten aluminium at 770° C under static conditions, Komatsu *et al.* [4] weighed the solid specimens and measured their dimensions to control the rate of the process. The aluminium alloys obtained were not analysed for the contents of dissolved elements. Therefore, it is impossible to establish from their data whether the dissolution of stainless steel in liquid aluminium was selective or non-selective in nature. The first aim of the present work was to answer this question. The second was to study the composition and growth kinetics of the intermetallic layers at the stainless steel–aluminium interface. These data are of interest for some technological applications, especially in making steel-to-aluminium transition joints and hot-dip aluminizing.

2. Experimental procedure

2.1. Materials

A classical 18Cr–10Ni stainless steel containing 70 ± 1% Fe, 18.0 ± 0.5% Cr, 10.5 ± 0.2% Ni and 0.08 ± 0.01% C was used for this investigation. The main inpurities were 1.2% Mn, 0.58% Ti, 0.64% Si, 0.22% Cu, 0.032% P and 0.003% S.

Two kinds of aluminium were used. The first was high-purity aluminium: 99.995% Al, the impurities being iron, titanium, silicon, copper and zinc

0022–2461/90 $03.00 + .12 © *1990 Chapman and Hall Ltd.*

$\geq 0.001\%$ each. The second was commercially pure aluminium containing 99.3 ± 0.1% Al, 0.24 ± 0.01% Fe, 0.003 ± 0.001% Cr and 0.005 ± 0.001% Ni, the other impurities being mainly 0.3% Si and 0.1% Zn.

2.2. Specimens

Cylindrical steel specimens, 11.28 ± 0.01 mm diameter and 5 to 6 mm high, were machined from 12 mm diameter rods. The disc surfaces were then ground and polished mechanically.

Immediately before the experiment the steel specimen was rinsed in ethanol and dried. It was then pressed into a high-purity graphite tube, 16.0 ± 0.2 mm diameter, to protect its lateral surface from the melt. Therefore, only the disc surface dissolved during the run. The specimen surface area exposed to the liquid aluminium attack was 1 cm^2. Where a greater surface area was desirable while its instantaneous value was unimportant, steel specimens with unprotected lateral surfaces were used. In such cases the graphite tubes served only as holders for the steel specimens.

2.3. Methods

The rapid-quenching device employed in this work has been described in detail elsewhere [5]. The experiments were performed mainly by the rotating disc technique. The experimental procedure differed very little from that described in the previous work [6]. A schematic diagram to illustrate the run is given in Fig. 1.

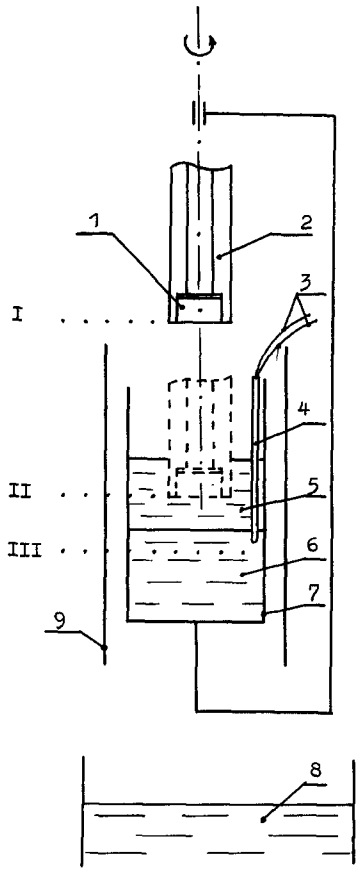

Figure 1 Schematic diagram to illustrate the experiment. 1, Stainless steel specimen; 2, graphite protective tube; 3, chromel–alumel thermocouple; 4, alumina protective tube; 5, flux; 6, liquid aluminium; 7, alumina crucible; 8, water bath; 9, furnace.

A special flux composed mainly of the alkali halides was used both to protect the aluminium melt from oxidation and to pre-heat the specimen to the required temperature. The flux was first melted in a 26 mm i.d. alumina crucible. Melting began at about 350° C. Pieces of aluminium were then melted under a flux. When the required temperature had been reached, the rotating steel specimen was lowered from position I into position II (Fig. 1) near the middle of the flux layer. During pre-heating, the distance between the disc surface and the liquid aluminium surface was about 10 mm. When the temperature had equilibrated (typically after 500 sec) the specimen, rotating at the required speed, was lowered from position II into position III in the bulk of liquid aluminium, so that the distance between the disc surface and the crucible bottom was 15 ± 0.5 mm. This was the beginning of the run. The disc was allowed to rotate in the aluminium melt for a pre-determined period of time. The temperature of the liquid phase was measured by a chromel–alumel thermocouple. During the run, its deviations from the required value were 2 to 5° C. The run was then ended in one of the two following ways.

1. When studying the dissolution process, the steel specimen was lifted from position III into position II and the crucible, together with the melt, the flux and the specimen, was allowed to cool in a water bath. After cooling, the major portion of the aluminium alloy adhering to the steel surface was removed mechanically. The remainder was dissolved in a 20% aqueous solution of NaOH. The steel specimen, free of both aluminium and intermetallic layers, was then washed with water and alcohol, dried and weighed. Because the specimen had also been weighed before the run, its mass loss during dissolution in liquid aluminium could be determined.

Samples of aluminium alloys obtained were analysed to determine their iron, chromium and nickel contents by photometric methods. The relative error in determination did not exceed 10% for iron, 25% for chromium and 40% for nickel.

2. When studying the growth kinetics of the intermetallic layers, the crucible, together with the flux, the melt and the steel specimen, was "shot" into water to arrest the reactions at the steel–aluminium interface. It should be emphasized that the specimen continued to rotate until solidification of the melt. It took typically 2 sec to cool an experimental cell from the investigation temperature to room temperature.

After cooling, the bimetallic specimen obtained was cut along the cylindrical axis, ground flat and polished electrolytically using a "Elypovist" electropolishing apparatus and special electrolytes [7]. The cross-sections prepared in such a way were examined metallographically. Microhardness measurements were also made. Concentration profiles of aluminium, iron, chromium and nickel in the reaction zone were recorded using a Jeol-Superprobe 733 microanalyser operating at 25 kV. In addition, the values of concentration of those elements near the middle part of the intermetallic layers and in the bulk of both steel and

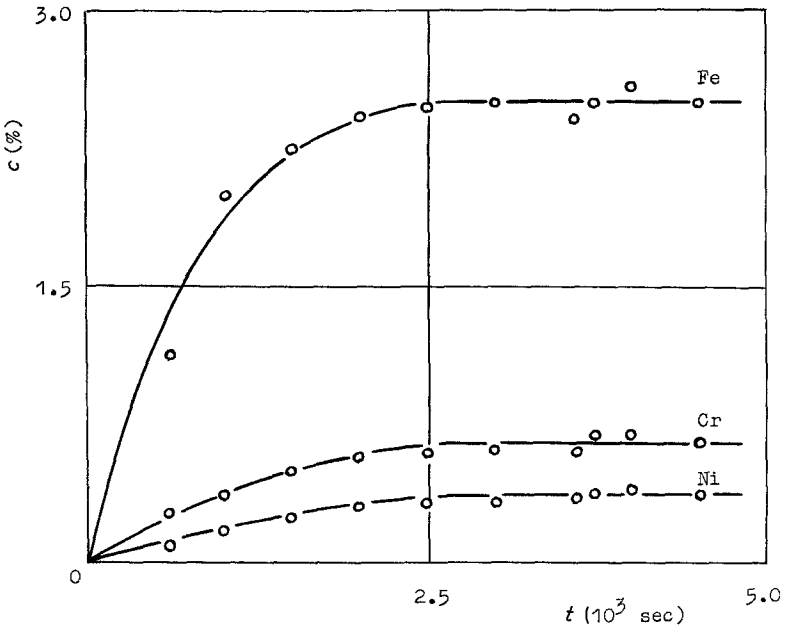

Figure 2 Concentration–time relationships for iron, chromium and nickel undergoing dissolution from the steel into liquid aluminium. Temperature = 700° C; rotational speed, ω = 54.0 rad sec^{-1}.

aluminium were determined by electron probe microanalysis. An attempt has also been made to define the composition of the intermetallic layers by X-ray techniques.

3. Results and discussion

3.1. Dissolution kinetics

It is well known that the dissolution of a solid metal in a liquid metal is usually described by the equation (see, for example, [1, 2, 5, 6, 8])

$$\frac{dc}{dt} = k\frac{S}{v}(c_s - c) \quad (1)$$

which in the integrated form (initial condition: $c = 0$ at $t = 0$) becomes

$$c = c_s\left[1 - \exp\left(-\frac{kSt}{v}\right)\right] \quad (2)$$

where c is the concentration of the dissolved metal in the bulk of the melt (kg m^{-3}); t is the time (sec); c_s is the saturation concentration (kg m^{-3}); k is the dissolution rate constant (m sec^{-1}); S is the solid specimen surface area (m^2) and v is the melt volume (m^3).

Equation 2 can be written as

$$\ln\left(\frac{c_s}{c_s - c}\right) = k\frac{St}{v} \quad (3)$$

if the initial concentration of a solute in the melt is zero, or as

$$\ln\left(\frac{c_s - c_0}{c_s - c}\right) = k\frac{St}{v} \quad (4)$$

if this concentration is c_0.

The dissolution of pure iron as well as low alloyed steels in pure liquid aluminium and its melts containing small amounts of other elements follows Equations 1 to 4 [6, 9–11]. The stainless steel investigated in this work contained totally about 30% alloying elements and impurities. Therefore, it was necessary to check experimentally the applicability of Equations 1 to 4 in the case of such a relatively complex material.

3.1.1. Saturation concentrations

To find the saturation concentrations of iron, chromium and nickel from the steel in liquid aluminium, the unprotected steel specimens were dissolved in a

TABLE I Results of determination of the saturation concentrations of iron, chromium and nickel from the steel in liquid aluminium

Aluminium	Temperature (° C)	Time (sec)	Rotational speed (rad sec^{-1})	Concentration (%)					
				Fe		Cr		Ni	
				ML*	CA†	ML*	CA†	ML*	CA†
High-purity	700	4000	32.7	2.5	2.5	0.63	0.59	0.37	0.33
		4500	32.7	2.5	2.5	0.63	0.61	0.37	0.33
		3600	54.0	2.4	2.2	0.61	0.58	0.36	0.48
		4000	54.0	2.6	2.4	0.67	0.66	0.39	0.45
		4500	54.0	2.4	2.5	0.61	0.60	0.36	0.48
		3700	54.0	2.5	2.3	0.65	0.63	0.38	0.32
Commercial	700	3000	54.0	2.4‡	2.4	0.56	0.55	0.33	0.48
		3700	54.0	2.5‡	2.5	0.58	0.55	0.34	0.44
High-purity	850	2500	54.0	7.1	7.8	1.8	1.4	1.07	1.2
		3000	54.0	7.4	7.1	1.9	1.4	1.11	1.05
		3600	54.0	7.2	7.4	1.9	1.6	1.8	1.1

*Calculated from mass loss measurements on the assumption of non-selective dissolution of the steel in liquid aluminium.
†Obtained by chemical analysis.
‡Taking into account that the commercially pure aluminium contained initially 0.24% Fe.

TABLE II Saturation concentrations* of the elements from the steel into liquid aluminium and their solubilities in the aluminium–transition metal binary systems at 700 to 850° C

Temperature (° C)	Saturation concentration (%)			Solubility (%) [2]		
	Fe	Cr	Ni	Fe	Cr	Ni
700	2.5 ± 0.2	0.64 ± 0.03	0.37 ± 0.02	2.5	0.72	10.0
725	3.0 ± 0.2	0.78 ± 0.03	0.45 ± 0.02	–	–	–
750	3.4 ± 0.2	0.88 ± 0.04	0.52 ± 0.03	3.4	1.29	13.5
800	5.0 ± 0.2	1.3 ± 0.1	0.76 ± 0.05	5.3	2.5	19.5
850	7.2 ± 0.3	1.9 ± 0.1	1.10 ± 0.06	7.9	4.1	27.0

*Values obtained from mass loss measurements are given as more precise values compared to chemically determined ones.

liquid–metal bath until saturation of the melt was attained and the dissolution practically stopped, as shown in Fig. 2. Experimental data obtained in the regions of saturation concentrations at 700 and 850° C are given in Table I. As seen, the concentrations calculated from mass loss measurements on the assumption of non-selective dissolution of the steel in liquid aluminium are in good agreement with those obtained by chemical analysis of aluminium alloys after the runs [12]. The values of saturation concentrations are listed in Table II [13]. The solubilities in binary systems taken from the work by Yeremenko *et al.* [2] are also given for comparison. Note that the saturation concentration of iron from the steel into liquid aluminium at 700° C coincide with its solubility in the Al–Fe binary system, both values being 2.5%. The saturation concentration of chromium (0.64%) is somewhat less than its solubility in the Al–Cr binary system (0.72% [2]), whereas the saturation concentration of nickel (0.37%) is far less than its solubility in the Al–Ni binary system (10%). The same is also observed at 725 and 750° C, whereas at 800 and 850° C there is a slight influence of chromium and nickel on the saturation concentration of iron in liquid aluminium.

3.1.2. Ratios of concentrations of elements during dissolution of steel in high-purity aluminium melts

The experimental data obtained at 700° C are presented in Table III. Values of iron, chromium and nickel concentrations in the melt found mainly by chemical analysis of aluminium alloys are given.

The ratio, C_{Fe}/C_{Cr}, of iron to chromium content into the steel is 3.9. If the dissolution of the steel in liquid aluminium is non-selective, then the ratio, c_{Fe}/c_{Cr}, of iron to chromium concentration in the melt should be the same. The limits set by experimental errors are ± 1.1. Thus, the ratio c_{Fe}/c_{Cr} in the melt should be 3.9 ± 1.1, as confirmed in Table III.

The ratio, C_{Fe}/C_{Ni}, of iron to nickel content is 6.7. Under conditions of non-selective dissolution the ratio c_{Fe}/c_{Ni} in the melt should be 6.7 ± 3.0. As is seen from Table III, this is in fact the case.

3.1.3. Ratios of concentrations of elements during dissolution of steel in commercial aluminium melts

The experimental data on the dissolution kinetics of the steel in the commercially pure aluminium melts are given in Table IV. The values of iron concentrations in Table IV are mainly the chemically determined ones, from which 0.24% was subtracted because the commercially pure aluminium contained initially 0.24% Fe.

As seen from Table IV, the experimentally determined values of c_{Fe}/c_{Cr} and c_{Fe}/c_{Ni} ratios are in fairly good agreement with the expected values of 3.9 ± 1.1 and 6.7 ± 3.0, respectively. Thus, the dissolution of the steel into both high-purity and commercially pure aluminium melts is non-selective.

3.1.4. Dissolution rate constants

To find exact values of the dissolution rate constants, the initial parts of the dissolution curves were thoroughly investigated. The concentrations of iron from the steel in the melts are plotted against St/v in Fig. 3.

TABLE III Experimental data on the dissolution kinetics of the steel in the high-purity aluminium melts. Temperature = 700° C; rotational speed, $\omega = 24.0\,\text{rad sec}^{-1}$; $S/v = 10\,\text{m}^{-1}$

Time (sec)	Concentration (%)			Ratio of concentrations in the melt		k (10^{-5} m sec^{-1})
	Fe	Cr	Ni	c_{Fe}/c_{Cr}	c_{Fe}/c_{Ni}	
100	0.12	0.040	0.025	3.0	4.8	4.9
150	0.18	0.046	0.034	3.9	5.3	5.0
200	0.22	0.050	0.039	4.4	5.6	4.6
300	0.33	0.080	0.050	4.1	6.6	4.7
400	0.45	0.12	0.050	3.8	9.0	5.0
500	0.50	0.12	0.11	4.2	4.5	4.5
550	0.60	0.16	0.091	3.8	6.6	4.9
600	0.60	0.14	0.10	4.3	6.0	4.6
650	0.71	0.16	0.10	4.4	7.1	5.1
650	0.71*	–	–	–	–	5.1
750	0.81*	–	–	–	–	5.2
1100	1.07*	–	–	–	–	5.1

*Values calculated from mass loss measurements.

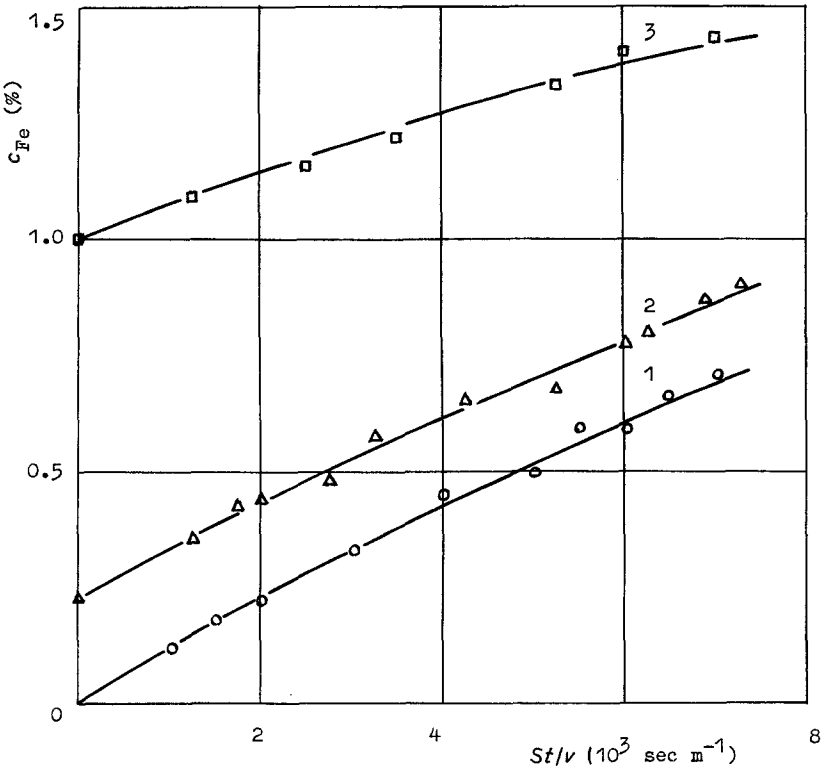

Figure 3 Concentration of iron from the steel plotted against St/v. Temperature = 700° C; ω = 24.0 rad sec^{-1}; S/v = 10 m^{-1}. 1, High-purity aluminium; 2, commercially pure aluminium; 3, Al + 1% Fe from the steel.

To find v, it is necessary to know the density of the aluminium melts containing various amounts of alloying elements, up to 10% Fe, Cr and Ni in total. Owing to the lack of these data in the literature, the density of the aluminium melts, ρ_{Al}, was assumed to be constant up to the saturation concentrations at all temperatures under investigation, $\rho_{Al} = 2.4 \times 10^3$ kg m^{-3} [14, 15]. Such an approximation seems at first sight to be very rough and unjustified. However, this is not the case. It is easy to estimate that even at 850° C the density of the saturated melts should not differ from that of pure liquid aluminium by more than 0.2×10^3 kg m^{-3}. This is about 8% of the mean value. Therefore, the relative error of determination of the dissolution rate constant introduced under such an assumption is 4% [16]. It is clearly less at lower temperatures. In the present case this level of inaccuracy appears to be acceptable.

Thus, in this work the volume of the melt was assumed to be constant during the whole course of dissolution of the steel in the aluminium melts, v = 10 cm^3. It is clear that in such a case the concentrations of the solutes could be expressed in mass % instead of kg m^{-3} which would facilitate calculations.

If the dissolution run follows Equations 1 to 4, then a plot of ln $[(c_s - c_0)/(c_s - c)]$ against St/v should be a straight line, as confirmed in Fig. 4. Experimental values of the dissolution rate constants are listed in Tables III and IV. The mean values of the dissolution rate constant at 700° C and a rotational speed of 24.0 rad sec^{-1} obtained by the least-squares fit method are:

(i) $k = (4.8 \pm 0.2) \times 10^{-5}$ m sec^{-1} for the high-purity aluminium melts;

(ii) $k = (4.6 \pm 0.3) \times 10^{-5}$ m sec^{-1} for the commercially pure aluminium melts;

(iii) $k = (4.8 \pm 0.3) \times 10^{-5}$ m sec^{-1} for the aluminium melts containing 1% Fe from the steel.

An aluminium alloy containing 1% Fe and corresponding amounts of the other elements was prepared

TABLE IV Experimental data on the dissolution kinetics of the steel in the commerical aluminium melts. Temperature = 700° C; rotational speed, ω = 24.0 rad sec^{-1}; S/v = 10 m^{-1}

Time (sec)	Concentration (%)			Ratio of concentrations in the melt		k (10^{-5} m sec^{-1})
	Fe	Cr	Ni	c_{Fe}/c_{Cr}	c_{Fe}/c_{Ni}	
125	0.12	0.040	0.030	3.0	4.0	4.4
175	0.19	0.040	0.032	4.8	5.9	5.0
200	0.20	0.050	0.043	4.0	4.7	4.6
275	0.24	0.067	0.062	3.6	3.9	4.1
325	0.34	0.070	0.065	4.5	5.2	5.0
425	0.42*	–	–	–	–	4.8
525	0.44	0.11	0.097	4.0	4.9	4.1
600	0.52	0.12	0.10	4.3	5.2	4.4
600	0.54	0.11	0.090	4.9	6.0	4.6
625	0.56*	–	–	–	–	4.6
725	0.67*	–	–	–	–	4.9

*Values calculated from mass loss measurements.

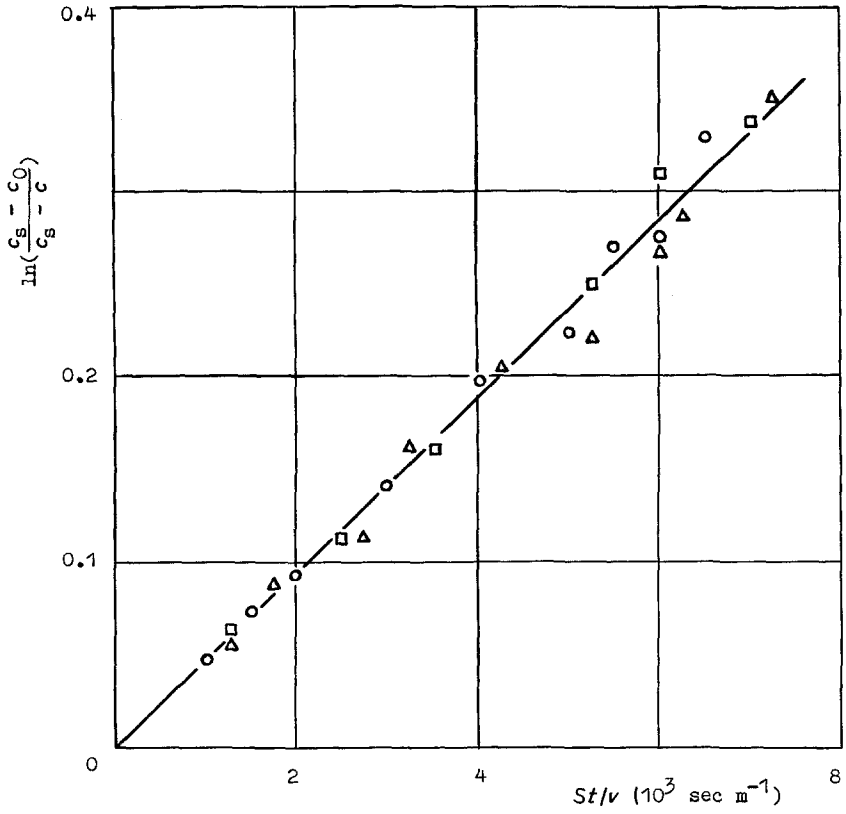

Figure 4 A plot of $\ln [(c_s - c_0)/(c_s - c)]$ against St/v for the data of Fig. 3.

by arc melting of the aluminium and the steel taken in appropriate amounts. Pieces of this alloy were then used as a starting melt material. As seen, there is no difference in dissolution rate constants for the three types of the aluminium melts investigated.

3.1.5. The effect of hydrodynamic conditions of flow of the liquid on the dissolution rate constant

It is well known that the dissolution rate of solids in liquids strongly depends on the intensity of liquid agitation. For a rotating disc, the dissolution rate constant, k, is related to the angular speed of rotation, ω, through the equation given by Levich [17]

$$k = 0.62 D^{2/3} \nu^{-1/6} \omega^{1/2} \quad (5)$$

where D is the diffusion coefficient of the solute across the diffusion boundary layer at the solid–liquid interface ($m^2 sec^{-1}$), and ν is the kinematic viscosity of the liquid phase ($m^2 sec^{-1}$). Equation 5 is valid only if the Schmidt number, $Sc = \nu/D$, exceeds 1000 [17]. Because for liquid–metal melts this number is usually much smaller, the Kassner equation which holds for $Sc \geqslant 4$ appears to be preferable

$$k = 0.554 I^{-1} D^{2/3} \nu^{-1/6} \omega^{1/2} \quad (6)$$

where $I = f(Sc)$ [18].

In addition to the runs performed at a rotational speed of 24.0 rad sec^{-1}, the dissolution rates of the steel in liquid aluminium were also measured at the following angular speeds of the disc rotation: 6.45, 9.00, 15.3, 32.7, 54.0 and 82.4 rad sec^{-1} [19]. The concentrations of iron in the melt are plotted against St/v for these seven rotational speeds in Fig. 5. As is seen from Fig. 6 where a plot of $\ln c_s/c_s - c$ against St/v is given for the data of Fig. 5, Equations 1 to 4 hold in the 6.45 to 82.4 rad sec^{-1} range of rotational speeds. Values of the dissolution rate constants obtained are given in Table V.

From Equations 5 and 6 it follows that at a constant temperature the dissolution rate constant, k, must linearly depend upon the square root of the angular speed of the disc rotation, $\omega^{1/2}$, if conditions of flow are laminar. A plot of k against $\omega^{1/2}$ is shown in Fig. 7. A linear dependence of k upon $\omega^{1/2}$ is evidence of a diffusion-controlled character of the steel dissolution in liquid aluminium.

3.1.6. The diffusion coefficient of iron from steel into liquid aluminium at 700° C

The diffusion coefficient of iron from the steel across the diffusion boundary layer into the bulk of liquid aluminium can clearly be calculated using Equations 5 and 6, if the values of k, ν and ω are known. The problem arises, however, due to the lack of data on the viscosity of the aluminium melts containing transition metals. In addition, the literature data even for pure liquid aluminium are very scattered. In the previous work [6] where the results of a study of the dissolution kinetics of pure iron in liquid aluminium were presented, the kinematic viscosity, ν, of pure liquid alu-

TABLE V Values of the dissolution rate constant and the diffusion coefficient at different angular speeds of disc rotation. Temperature = 700° C; $S/v = 10\,m^{-1}$)

ω (rad sec^{-1})	k (10^{-5} m sec^{-1})	D (10^{-9} m^2 sec^{-1})	D_{mean} (10^{-9} m^2 sec^{-1})
6.45	2.8 ± 0.2	2.1	2.1
9.00	3.4 ± 0.3	2.2	
15.3	4.2 ± 0.2	2.0	
24.0	4.8 ± 0.2	1.8	
32.7	6.2 ± 0.3	2.2	
54.0	8.6 ± 0.3	2.3	
82.4	10.3 ± 0.5	2.2	

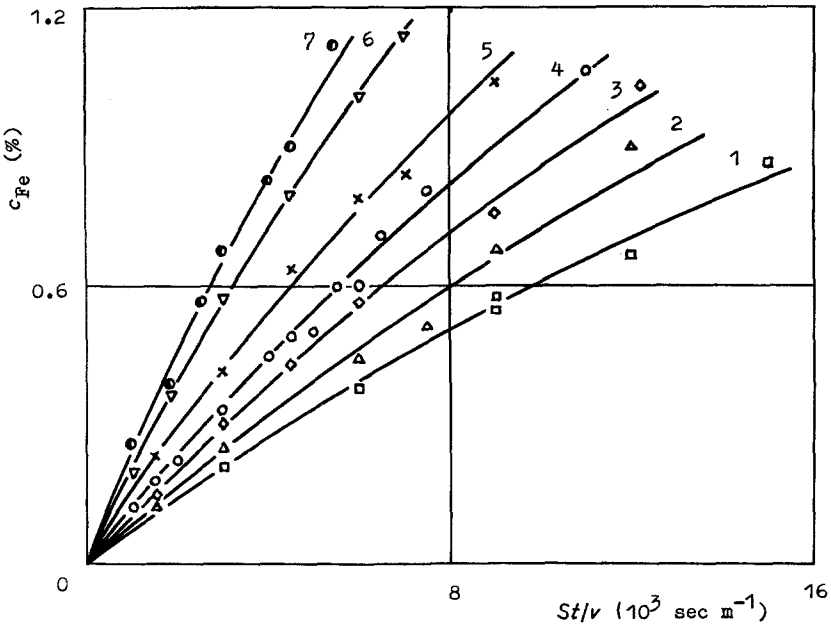

Figure 5 Concentration of iron from the steel in liquid aluminium plotted against St/v. Temperature = 700° C; S/v = 10 m^{-1}; rotational speed of discs: 1, 6.45; 2, 9.00; 3, 15.3; 4, 24.0; 5, 32.7; 6, 54.0; 7, 82.4 rad sec^{-1}.

minium at 700° C was adopted as 4.8×10^{-7} m^2 sec^{-1} from the data reported by Levin [20]. Niinomi *et al.* [21] used the following literature data: dynamic viscosity of pure liquid aluminium at 700° C, $\eta = 2.9 \times 10^{-3}$ kg m^{-1} sec^{-1}, and its density, $\rho_{Al} = 2.36 \times 10^3$ kg m^{-3}. Hence, in their work the kinematic viscosity, $\nu = \eta/\rho$, was adopted as 12.3×10^{-7} m^2 sec^{-1}, i.e. more than 2.5 times greater compared to that used previously [6].

From the data compiled by Vol [14] it may be concluded that each additional per cent of iron in the aluminium melt increases its dynamic viscosity by about 10%. The kinematic viscosity also increases, but to a lesser extent due to an increase in the melt density with increasing iron content. Assuming similar effects of both chromium and nickel on the viscosity of the melt it may be supposed that at 700° C its value should not differ from that for pure aluminium by more than 35% because at this temperature the total concentration of iron, chromium and nickel in the saturated melt is 3.5 ± 0.2%. In view of the low accuracy of viscosity measurements this difference appears to be insignificant. Therefore, here the same value, $\nu = 4.8 \times 10^{-7}$ m^2 sec^{-1}, of the melt viscosity as in the previous work [6] was used for calculations. At least, this permits a comparison of the results obtained with the use of pure iron and stainless steel to be made.

Fortunately, large variations in the viscosity values have comparatively little influence on the calculated diffusion coefficient because the dissolution rate constant is related to a small power of the viscosity, that being only −1/6 (see Equations 5 and 6). Immediate calculations show that the three-fold increase in the viscosity value changes the value of the diffusion coefficient by about 30%.

The approximate value of the diffusion coefficient, D, was first calculated from Equation 5; the Schmidt number, Sc, and the correction factor, I [18], were then

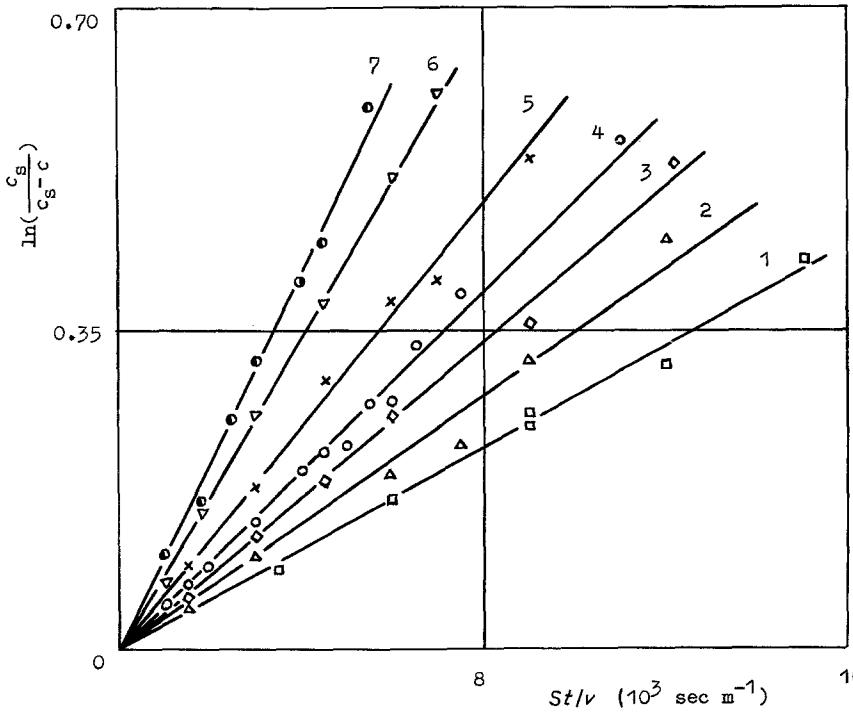

Figure 6 A plot of ln $[c_s/(c_s - c)]$ against St/v for the data of Fig. 5.

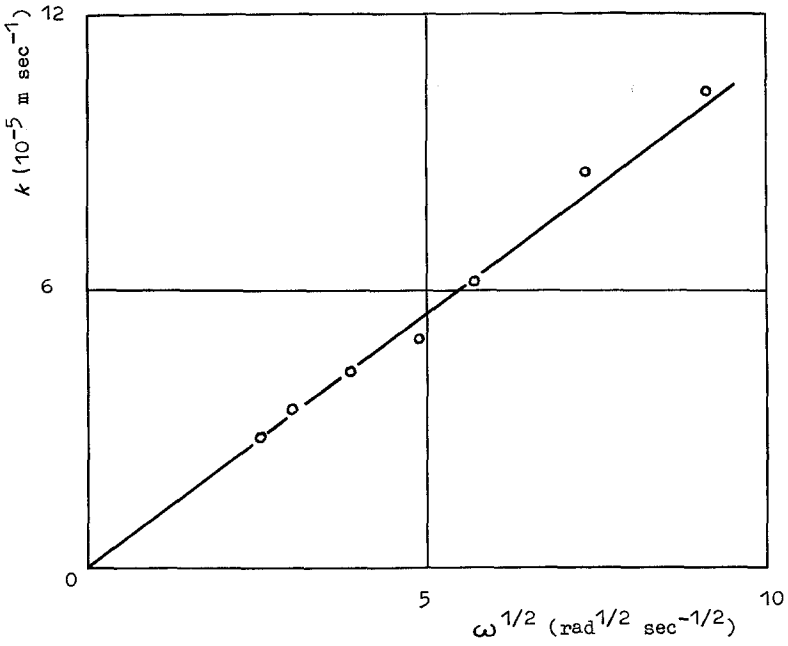

Figure 7 A plot of k against $\omega^{1/2}$ at a temperature of 700° C.

found, and the final value of D was calculated from Equation 6. Values of the diffusion coefficient of iron from the steel across the diffusion boundary layer into liquid aluminium are listed in Table V. At 700° C the mean value is 2.1×10^{-9} m^2 sec^{-1}. The relative error of its estimation appears to be less than $\pm 30\%$. About two-thirds of this value is due to the uncertainty in viscosity of the melt.

In the case of pure iron dissolution in liquid aluminium the diffusion coefficient of iron is 1.24×10^{-9} m^2 sec^{-1} [6]. This is in agreement with the corrosion tests by Komatsu *et al.* [4] who found a stainless steel to be less resistant to the liquid aluminium attack compared to low alloyed steels and some other ferrous alloys.

It should be emphasized that the above value, $D = 2.1 \times 10^{-9}$ m^2 sec^{-1}, is the diffusion coefficient not only for iron diffusion from the steel into the melt, but for both chromium and nickel diffusion as well. Because the steel dissolution in liquid aluminium is non-selective, all its constituents pass across the diffusion boundary layer at the steel–aluminium interface at equal rates. Thus, the steel behaves likes a single element during its dissolution into the aluminium melts.

3.1.7. The temperature dependence of the dissolution rate constant

The temperature dependence of the dissolution rate constant was investigated at a rotational speed of 24.0 rad sec^{-1}. In addition to a temperature of 700° C, dissolution runs were also made at 725, 750, 800 and 850° C. The iron concentrations from the steel into the melt are plotted against St/v in Fig. 8. These

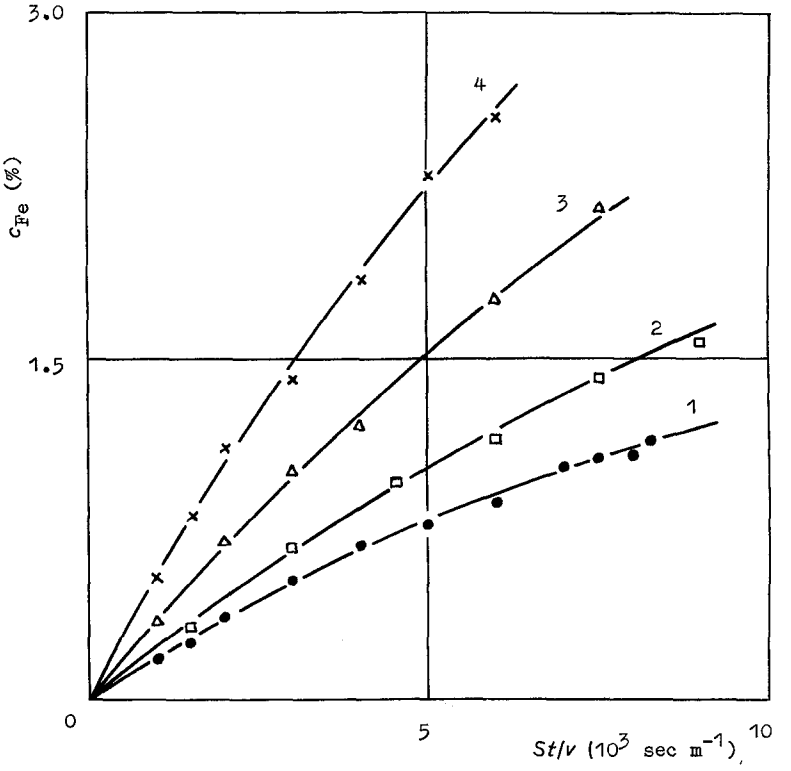

Figure 8 Concentration of iron from the steel into the aluminium melt plotted against St/v. Rotational speed, $\omega = 24.0$ rad sec^{-1}; $S/v = 10$ m^{-1}. 1, 725° C; 2, 750° C; 3, 800° C; 4, 850° C.

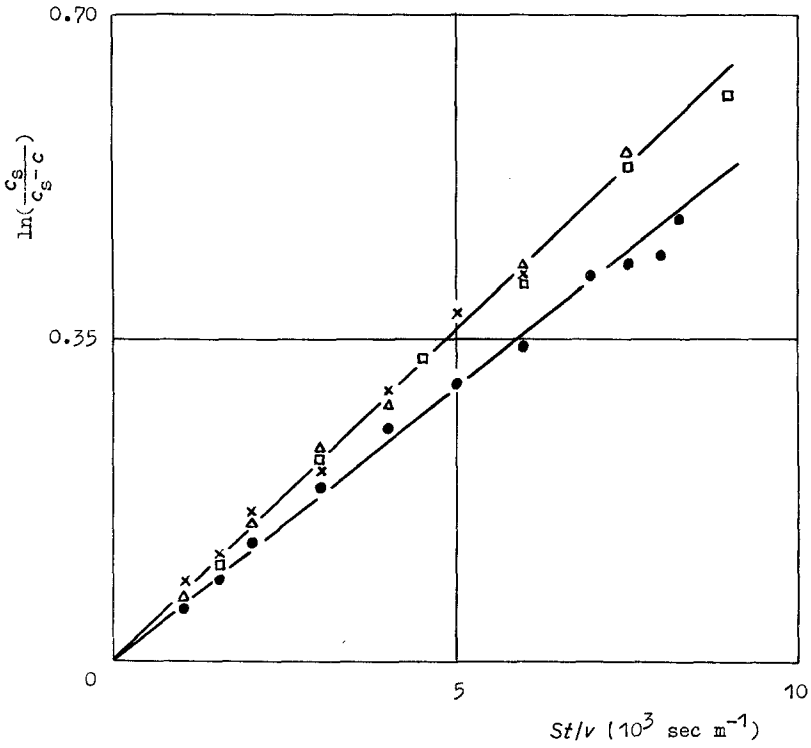

Figure 9 A plot of $\ln [c_s/(c_s - c)]$ against St/v for the data of Fig. 8.

relationships seem at first sight to be quite usual, because at a constant time the iron concentrations in the melt gradually increase with increasing temperature.

However, there is an interesting feature distinguishing the steel dissolution in liquid aluminium from the transition metal (Fe, Cr, Ni, etc.) dissolution. This can be revealed by plotting $\ln c_s/c_s - c$ against St/v as shown in Fig. 9. As seen from Fig. 9 and Table VI, where the experimental values of the dissolution rate constant at 725 to 850° C are listed, the dissolution rate constant remains almost unchanged in the range of temperatures from 750 to 850° C. At least, at 800° C it is exactly the same as at 850° C.

When the transition metal (Fe, Cr, Ni, Ti, etc.) alone is dissolved in the aluminium melt, the temperature dependence of its dissolution rate constant, k, usually obeys an equation of the Arrhenius type: $k = k_0 \exp(-E/RT)$, where E is the activation energy, R is the gas constant and T is the absolute temperature [1, 2, 5]. Clearly, this does not hold in the case of steel dissolution in the aluminium melt.

Why the dissolution rate constant remains constant with increasing temperature can be explained, at least qualitatively, on the basis of Equations 5 and 6. Indeed, there are two temperature-dependent quantities in these equations, namely, the diffusion coefficient, D, of iron from the steel into the melt, and the viscosity, v, of the melt, the effect of temperature on I [18] being negligible. While increasing the temperature by itself results in a decrease in the melt viscosity, the simultaneous increase of the transition metal content of the saturated melt (see Table II) causes its sharp increase with temperature. Therefore, even the two-fold difference in viscosity of the melt at 850° C compared to that at 800° C appears to be probable. Such a difference in viscosities causes a decrease in k by about 12%. Again, increasing the temperature from 800 to 850° C results in an increase of the transition metal (Fe, Cr, Ni, Ti, etc.) diffusion coefficient into the aluminium melt by 10 to 25%, that being about 15% for iron, 17% for chromium and 12% for nickel [2]. In view of the noticeable mutual influence of the steel constituents on their saturation concentrations at higher temperatures (see Section 3.1.1 and Table II), a similar effect might also be expected for the diffusion coefficient that would lead to its less pronounced temperature dependence. Probably, a change in value of the diffusion coefficient, D, with increasing temperature is compensated by a change in value of the melt viscosity, v, as these act in opposite directions, so that the product $(D^{2/3}v^{-1/6})$ and, in turn, the dissolution rate constant, k, in Equations 5 and 6 remains the same at both 800 and 850° C. In view of this fact, it is not improbable that a value of the dissolution rate constant may be even less at a higher temperature than that at a lower one.

Clearly, this consideration is purely speculative. No quantitative proof can be offered, because viscosity data for the transition metals containing aluminium melts are lacking. Further experimental work in this field is needed.

TABLE VI Values of the dissolution rate constant at 725 to 850° C. Rotational speed, $\omega = 24.0$ rad sec^{-1}; $S/v = 10$ m^{-1}

Temperature (° C)	k (10^{-5} m sec^{-1})	Temperature (° C)	k (10^{-5} m sec^{-1})
725	5.8 ± 0.2	800	7.3 ± 0.4
750	7.1 ± 0.3	850	7.3 ± 0.6

3.2. Growth of the intermetallic layers in the case of a saturated melt

An aluminium alloy containing 2.5 ± 0.2% Fe and corresponding amounts of other steel constituents was previously prepared by arc melting the appropriate

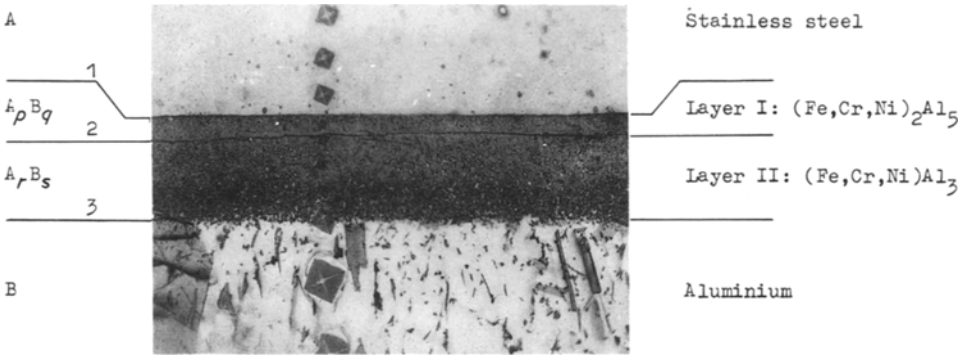

Figure 10 Micrograph of the steel–aluminium reaction zone. Temperature = 700° C; time = 3000 sec; melt: Al + 2.5% Fe from the steel. ×440.

amounts of high-purity aluminium and steel shavings under an argon atmosphere [22]. Pieces of this alloy were then used for the investigation. The temperature of the melt was 700° C. Because the melt had been saturated with respect to the steel constituents, no dissolution of the steel could clearly occur during the run at this temperature.

Two intermetallic layers were found to form during interaction of the 18Cr–10Ni stainless steel specimens with the saturated aluminium melts for 100 to 3600 sec. A typical micrograph of the steel–aluminium reaction zone is shown in Fig. 10. The layer (Layer I) adjacent to the steel was compact, while that (Layer II) adjacent to the melt material was porous. The thickness of Layer II was a few times greater than that of Layer I (see Fig. 10 and Table VII). The relative error in layer thickness measurements was 10% to 25%. Metallographic examination of specimen cross-sections showed a microstructure of the steel base to be homogeneous until its interface with Layer I. The aluminium part of the bimetallic specimens contained inclusions of intermetallic phases, as seen in Fig. 10.

It is well known that of five compounds existing in the Fe–Al binary system [14, 23], usually only two, namely Fe_2Al_5 and $FeAl_3$, form intermetallic layers during interaction of iron and steels with aluminium and its alloys (see, for example, [4, 6, 11, 24]). These have close compositions: Fe_2Al_5 contains 54.7% Al and $FeAl_3$ contains 59.2% Al. Their physico-chemical properties are also similar. Therefore, these compounds are hardly distinguishable in intermetallic layers. It is not surprising that there are some discrepancies in results reported by different authors, even if pure elements were used for the study. If the alloys are used as starting materials, the difficulties with phase identification increase considerably because the system becomes multicomponent, as is the case in the present work.

TABLE VII Experimental values of thickness of the intermetallic layers at the interface between the steel surface and the saturated aluminium melt at 700° C

Specimen no.	Time (sec)	Thickness (μm)		Total thickness of both layers (μm)
		Layer I	Layer II	
22	5	0.2	3.5	3.7
23	100	3.5	11	14.5
20	225	4.5	15	19.5
24	400	5.7	17	22.7
26	900	6.8	18	24.8
43	1000	8	19	27
27	1600	8.6	25	33.6
42	2000	9.5	25	34.5
41	3000	10	34	44
40	3600	10	40	50

3.2.1. X-ray analysis

It was quite impossible to interpret the data obtained by X-ray powder techniques. Therefore, X-ray patterns of polished cross-sections were obtained with a 57.3 mm diameter camera using Cr$K\alpha$ or Cu$K\alpha$ radiation [25]. Fortunately, the bimetallic specimens where the intermetallic layers were thick enough (30 to 40 μm) could be easily broken along the boundary between Layers I and II. After slight mechanical polishing, the surfaces of both parts of the specimen were suitable for X-ray examination and the first two X-ray patterns were taken. Then, the cross-sections were again ground (if necessary) and polished to remove a little material and new X-ray patterns were taken. In total, one X-ray pattern of the aluminium matrix, two of Layer II in its different sections (about 5 and 15 μm away from the interface between Layers I and II), one of Layer I and one of the steel base were obtained using one bimetallic specimen.

Interplanar distances (d-spacing calculated from the Bragg equation) together with the relative line intensities are given in Table VIII. The literature X-ray data for Fe_2Al_5, $FeAl_3$, aluminium and γ-iron [26] are also presented for comparison. While the interplanar distances for Layer I are close to those for Fe_2Al_5 and the interplanar distances for Layer II are close to those for $FeAl_3$, it is not so easy to arrive at a definite conclusion concerning the composition of the layers for the following reasons.

(a) As is seen from the literature data presented in Table VIII, the number of d-spacings for the phases under investigation including, unfortunately, the most characteristic reflections, coincide or at least are very close.

(b) The literature data were obtained using pure equilibrated starting materials whereas the intermetallic layers in this investigation formed under non-equilibrium conditions and, in addition, contained considerable amounts of alloying elements (see the next section). This could cause a shift in the diffraction

TABLE VIII X-ray data

This investigation												Literature data: Mirkin [25]							
Steel base		Layer I		Layer II				Aluminium matrix		High-purity aluminium		γ-Fe (Mo$K\alpha$ radiation)		Fe_2Al_5 (Mo$K\alpha$ radiation)		$FeAl_3$ (Cr$K\alpha$ radiation)		Al (Mo$K\alpha$ radiation)	
				~5 μm from Layer I–Layer II interface		~15 μm from Layer I–Layer II interface													
d-spacing (nm)	Intensity	*d*-spacing (nm)	Intensity	*d*-spacing (nm)	Intensity	*d*-spacing (nm)	Intensity	*d*-spacing (nm)	Intensity	*d*-spacing (nm)	Intensity	*d*-spacing (nm)	Intensity	*d*-spacing (nm)	Intensity	*d*-spacing (nm)	Intensity	*d*-spacing (nm)	Intensity
0.208	vs	0.209	s	0.232	w	0.232	w	0.233	vs	0.233	vs	0.207	100	0.211	100	0.2339	m	0.233	100
0.202	m	0.206	vs	0.225	w	0.226	w	0.226	w	0.201	s	0.180	50	0.205	100	0.2256	w	0.202	40
0.180	vs	0.202	s	0.210	vw	0.224	m	0.218	vw	0.1426	s	0.126	32	0.194	10	0.2125	w	0.1430	30
0.1437	vw	0.198	w	0.206	s	0.216	vw	0.201	s	0.1218	vs	0.1081	32	0.190	8	0.2096	vs	0.1219	30
0.1269	vs	0.193	m	0.203	vs	0.213	m	0.1429	vs	0.1168	m	0.1018	4	0.184	3	0.2082	w	0.1168	7
0.1173	w	0.184	vw	0.200	vs	0.209	w	0.1261	vw					0.176	8	0.2063	w	0.1011	2
0.1169	w	0.179	vs	0.193	m	0.206	vs	0.1218	vs					0.170	2	0.2042	vs		
		0.174	vs	0.191	m	0.203	vs	0.1205	vw					0.163	2	0.2021	vs		
		0.159	vw	0.178	w	0.200	vs	0.1168	vs					0.159	3	0.1936	w		
		0.152	vw	0.176	w	0.195	w							0.155	2	0.1768	vw		
		0.1438	w	0.152	w	0.179	vw							0.1475	16	0.1449	m		
		0.1387	w	0.1471	w	0.176	w							0.1418	2	0.1433	m		
		0.1350	w	0.1444	m	0.1482	m							0.1390	10	0.1396	w		
		0.1306	vw	0.1415	vw	0.1445	m							0.1350	2	0.1348	w		
		0.1267	vs	0.1394	m	0.1430	m							0.1300	2	0.1291	m		
		0.1252	vw	0.1353	w	0.1403	s							0.1272	10	0.1265	m		
		0.1222	w	0.1339	vw	0.1381	vw							0.1240	8	0.1255	m		
		0.1211	m	0.1307	vw	0.1341	w							0.1212	16	0.1247	m		
		0.1189	w	0.1277	s	0.1303	w							0.1180	2	0.1231	m		
		0.1175	w	0.1268	s	0.1282	w							0.1145	2	0.1222	m		
		0.1161	vw	0.1254	s	0.1275	w									0.1203	w		
				0.1247	m	0.1266	w									0.1182	m		
				0.1223	vs	0.1255	vw									0.1171	m		
				0.1212	vs	0.1248	w												
				0.1199	w	0.1219	m												
				0.1180	m	0.1211	vs												
				0.1169	vw	0.1192	vw												
						0.1180	m												
						0.1168	w												
						0.1164	m												

*Cr$K\alpha$ radiation. Intensity: vs = very strong, s = strong, m = mean, w = weak and vw = very weak

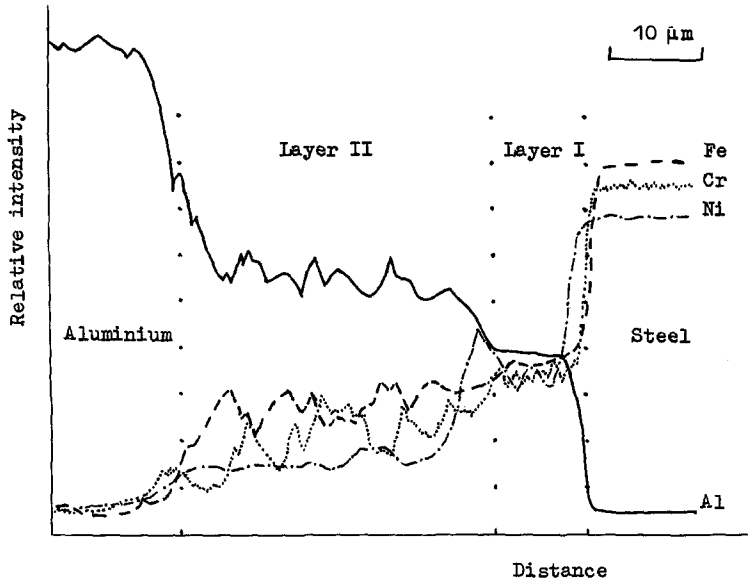

Figure 11 Concentration profiles of aluminium, iron, chromium and nickel in the reaction zone of a steel–aluminium bimetallic specimen. Temperature = 700° C; time = 3000 sec; melt: Al + 2.5% Fe from the steel.

peaks, line broadening, the disappearance of some reflections and the appearance of extra ones.

It is not surprising, therefore, that there was significant difference even in X-ray patterns taken from the same intermetallic layer (Layer II), but in its different sections (see Table VIII). No difference was revealed in X-ray patterns of the steel before and after the experiment. There was little difference in X-ray patterns of the aluminium matrix of bimetallic specimens and those of pure aluminium, due to the presence of intermetallic inclusions in the former (see Fig. 10).

3.2.2. Electron probe microanalysis

The concentration profiles of aluminium, iron, chromium and nickel in the reaction zone of the steel–aluminium specimen are shown in Fig. 11. The distribution of these elements in both the steel base and Layer I is almost uniform, whereas that in Layer II is very irregular. In addition, increasing the content of aluminium and a corresponding decrease in the content of iron, chromium and nickel with increasing distance away from the Layer I–Layer II interface is easily seen. Hence, Layer II had different compositions in its different sections. Probably, this is the main reason for the observed difference in its X-ray patterns (see Table VIII).

The contents of aluminium, iron, chromium and nickel, were determined by electron probe microanalysis near the middle of both Layer I and Layer II, in the steel base at a distance of 10 to 20 μm away from the Layer I–steel interface and in the aluminium matrix at a distance of 30 to 50 μm away from the Layer II–aluminium interface. Experimental values are listed in Table IX. It is seen that:

1. The steel composition found by electron probe microanalysis agrees fairly well with that found by chemical analysis before the experiment. Thus, no penetration of the liquid aluminium, nor the formation of a solid solution occurred during the run into the steel bulk.

2. Layer I contains 48.0% to 55.5% Al, 31.5% to 39.8% Fe, 5.0% to 9.2% Cr and 2.5% to 6.9% Ni. Its composition may presumably be expressed by the formula $(Fe, Cr, Ni)_2Al_5$.

3. Layer II contains 60.2% to 68.1% Al, 27.2% to 31.9% Fe, 2.9% to 4.3% Cr and 1.2% to 2.0% Ni. Its composition may presumably be expressed by the formula $(Fe, Cr, Ni)Al_3$ while it clearly contains excess aluminium. Here it is taken into account that excess aluminium is probably due to its inclusion in the free state in microsopic pores present in Layer II.

3.2.3. Microhardness measurements

A plot of microhardness, HV (20 g), against distance is given in Fig. 12. The microhardness of the steel base was the same, HV = 1.8 ± 0.2 GPa, at any point up to its interface with Layer I. Of all the phases investigated, Layer I had the highest microhardness, HV = 8.9 ± 0.9 GPa.

A gradual decrease (from HV = 4.5 GPa to HV = 3.06 GPa) of the microhardness within Layer II with increasing distance away from its interface with Layer I was observed. This was due to increasing amounts of aluminium inclusion in the same direction. The microhardness of the aluminium matrix was 0.6 ± 0.1 GPa.

3.2.4. "Paralinear" growth kinetics of the intermetallic layers

The variation of layer thickness with time plots are given in Fig. 13. It is seen that the thickness, x, of Layer I gradually increases in the time range 100 to 2000 sec and then remains constant, x_{max} = 10 μm. The thickness of Layer II, y, continuously increase with increasing dipping time. The kinetic curve of Layer II can clearly be divided into two pronounced regions. In the first region (0 to about 200 sec) its growth rate is almost twice that in the second region (t > 200 sec). It is difficult to establish the layer-growth kinetic law in the first region, while in the second it is clearly linear. Accordingly, the total thickness–time dependence also consists of two regions with different growth rates.

It should be emphasized that the "diffusional" theory in any modification gives no (even qualitative) explanation of such a relationship. It can only be

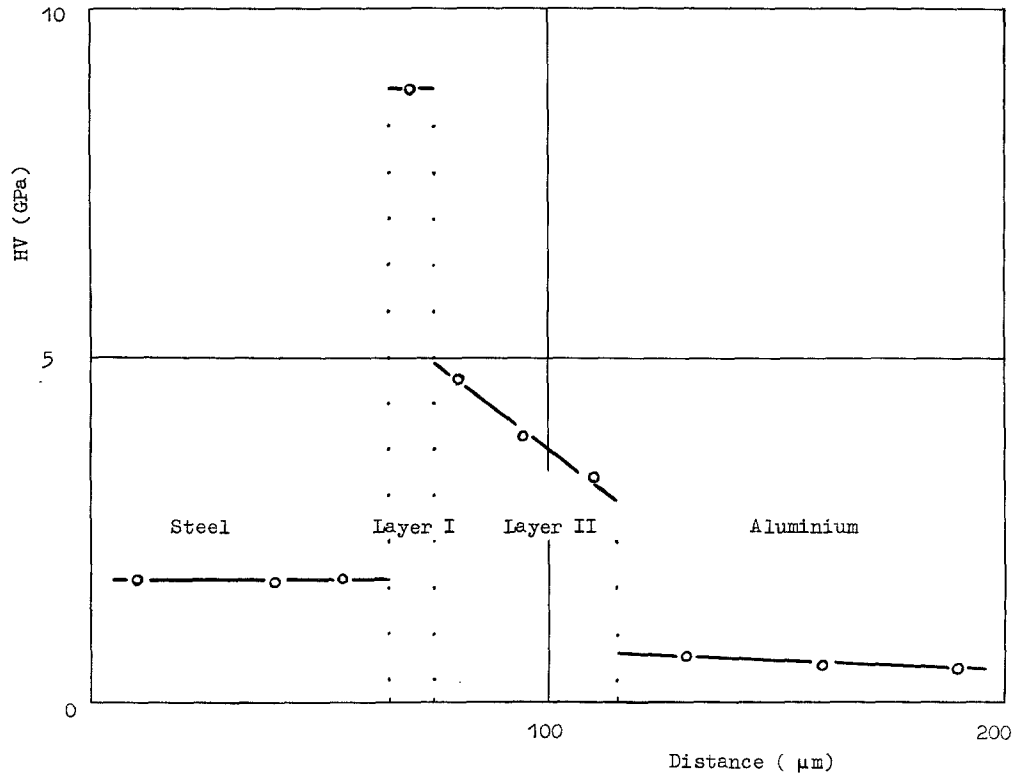

Figure 12 Microhardness HV (20 g) plotted against distance.

understood in terms of the "paralinear" growth kinetics (see, for example, [27, 28]).

While a few elements diffuse from the steel bulk across Layer I, it is the slowest diffusing element (probably iron) that plays a decisive role in determining the overall layer-growth rate. Let this element be A, $(Fe, Cr, Ni)_2Al_5$ be A_pB_q, $(Fe, Cr, Ni)Al_3$ be A_rB_s and aluminium be B (see Fig. 10). Then, the formation of the intermetallic layers can be represented by the following scheme [25, 28].

Layer Interface		Chemical Reaction	
A_pB_q	1	$qB + pA = A_pB_q$	(7)
	2	$(sp - qr)A + qA_rB_s = sA_pB_q$	(8)
A_rB_s	2	$(sp - qr)B + rA_pB_q = pA_rB_s$	(9)
	3	$rA + sB = A_rB_s$	(10)

First both layers grow at the expense of both components (A and B). Then, the regime of growth of the A_pB_q layer probably becomes diffusional with regard to component A and therefore the A_rB_s layer loses a source of A atoms (for details, see [28]). As a result, its growth rate must decrease almost twice, in accordance with the experiment.

"Paralinear" growth kinetics are observed, if the regime of the A_pB_q layer growth is diffusional with regard to both components A and B, whereas the regime of the A_rB_s layer growth is kinetic with regard to component B. Note that in this case the A_rB_s layer grows only at the expense of component B (Reaction 10 does not proceed), while the A_pB_q layer grows at the expense of both components. "Paralinear" growth

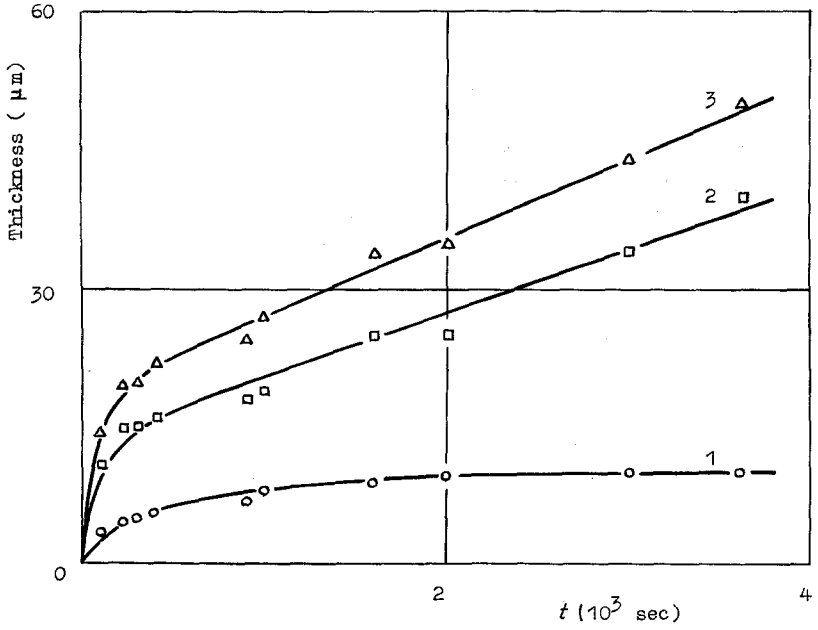

Figure 13 Layer thickness against dipping time plots. Temperature = 700° C; melt: Al + 2.5% Fe from the steel. 1, Thickness of Layer I; 2, thickness of Layer II; 3, total thickness of both layers.

kinetics follow the equations

$$\frac{dx}{dt} = \frac{k_{1B1} + k_{1A2}}{x} - \frac{rg}{p} k_{0B2} \quad (11)$$

$$\frac{dy}{dt} = k_{0B2} \quad (12)$$

where k_{1B1} and k_{1A2} are the physical (diffusional) constants ($m^2 sec^{-1}$), k_{0B2} is the chemical constant ($m sec^{-1}$) and g is the ratio of the molar volume of A_pB_q to that of A_rB_s [28].

The equations of this type were first proposed by Loriers (see Kofstad [27]) to describe the growth rates of two oxide layers. It should be noted that they follow in one of the limiting cases from a general system of differential equations given by Dybkov [28]. From Equation 11 it follows that the A_pB_q layer thickness, x, tends with time to a limiting value which can be found by putting $dx/dt = 0$; thus

$$x_{max} = \frac{(k_{1B1} + k_{1A2})p}{rgk_{0B2}} \quad (13)$$

The A_rB_s layer growth in the 900 to 3600 sec time range was found to be linear: $y = 1 \times 10^{-8} t + 6 \times 10^{-6}$ m. Therefore, $k_{0B2} = 1 \times 10^{-8}$ m sec^{-1}. Exact values of p, r and g are clearly unknown, due to the uncertainties in phase compositions of the layers. Using the experimental value $x_{max} = 10\,\mu m$, the sum $(k_{1B1} + k_{1A2})$ can, therefore, only be estimated assuming the molar volume of (Fe, Cr, Ni)$_2$Al$_5$ and (Fe, Cr, Ni)Al$_3$ to be equal to that of Fe_2Al_5 and $FeAl_3$, respectively. The latter quantities can be found using the values of the density of the compounds: $\rho_{Fe_2Al_5} = 4.1 \times 10^3$ kg m^{-3} [29] and $\rho_{FeAl_3} = 3.8 \times 10^3$ kg m^{-3} [14]. Thus, $V_{Fe_2Al_5} = 6.0 \times 10^{-5}$ m^3 mol^{-1} and $V_{FeAl_3} = 3.6 \times 10^{-5}$ m^3 mol^{-1}. Therefore, $g = 1.7$. Then, from Equation 13 it follows that ($p = 2$, $r = 1$) $k_{1B1} + k_{1A2} = 0.8 \times 10^{-13}$ m^2 sec^{-1}.

It should be emphasized that the initial parts of the x–t and y–t dependences are in general not parabolic. Nevertheless, a certain initial part of the total thickness–time dependence is close to a parabola. In the case under consideration this part (the 0 to about 400 sec time range) could be described with fairly good accuracy by the equation: $x^2 = 2k_p t$, where $k_p = (8 \pm 2) \times 10^{-13}$ m^2 sec^{-1}. From a formal view-point, it can therefore be concluded (especially when only the dependence of the total thickness or mass of both layers upon time is analysed) that the parabolic-growth law simply gradually transforms into the linear-growth law whereas the layer-growth kinetics are, in fact, more complicated.

3.3. Growth of the intermetallic layer in the case of an undersaturated melt

The runs were performed at 700° C for 100 to 600 sec. The rotational speed of discs was 24.0 rad sec^{-1}. The melts of both high-purity aluminium and commercial aluminium were used. In contrast to the case of a saturated melt, the single-phase intermetallic layers, 3 to $\sim 11\,\mu m$ thick, were metallographically found to form in both cases.

An attempt was made to define the phase composition of the intermetallic between the steel and the melt materials by electron probe microanalysis because this could not be done by other available means. Unfortunately, this method also produced poorer results compared to the case of a saturated melt, as can be seen from Table X. The most probable reason for this is that in the case of a brittle, very hard and, in addition, very thin intermetallic layer positioned between the relatively soft materials (the steel and aluminium alloys) it is difficult to prepare a flat polished surface. As a result, a certain amount of the radiation is not recorded, leading to underestimated contents of the elements. As seen from Table X, the sum of the contents of the elements (aluminium, chromium, iron and nickel) in the layer is less than 100%, the difference being -7.4 to -15.2%. It is therefore impossible to distinguish between the (Fe, Cr, Ni)$_2$Al$_5$ and (Fe, Cr, Ni)Al$_3$ phases.

Values of iron, chromium and nickel contents in the steel obtained by electron probe microanalysis after the runs (Table X) are in good agreement with those found by chemical analysis before the runs (see Section 2.1). This is further evidence for the non-selective character of the steel dissolution in the aluminium melts because in the opposite case a change in steel composition would clearly be observed.

A plot of layer thickness against time is given in Fig. 14. As seen, the intermetallic layer thickness continuously increases with increasing dipping time. There is no noticeable difference in layer-growth rates in cases where different initial melt materials (high-purity aluminium and commercial aluminium) were used. This is due, firstly, to the large scatter of experimental results (Fig. 14) and, secondly, to a small difference of the layer-dissolution rates, that being less than 10% (this is easily seen from Equation 2).

Unfortunately, due to the lack of necessary data, it is impossible to treat the experimental results presented here by the use of equations describing the layer-growth kinetics under conditions of its simultaneous dissolution [5, 6, 30]. No attempt was made to establish a so-called kinetic law of the layer growth by fitting the results according to a linear, parabolic, logarithmic or any other relation. Even if established, such a "law" would be clearly valid only under the dissolution conditions investigated and its applicability would, therefore, be very limited.

3.4. Making the steel-to-aluminium transition joints

The welding of aluminium to stainless steel meets serious difficulties, because these two materials represent one of the numerous examples of the so-called incompatible combinations [31, 32]. Therefore, the transition joints are often used in practice to connect dissimilar metals. A transition joint (or piece) is a relatively small bimetallic section – pipe, plate, etc. [31]. In use, like material is welded to like, by the usual techniques. In such a way, a bimetallic section with desirable dimensions can be obtained. The problem of joining dissimilar materials is thus eliminated. The problem of making the transition pieces clearly remains.

TABLE IX Data of electron probe microanalysis of contents obtained for a saturated aluminium melt

Specimen no.	Dipping time (sec)	Steel base				Layer I				Layer II				Aluminium matrix			
		Al (%)	Fe (%)	Cr (%)	Ni (%)	Al (%)	Fe (%)	Cr (%)	Ni (%)	Al (%)	Fe (%)	Cr (%)	Ni (%)	Al (%)	Fe (%)	Cr (%)	Ni (%)
40	3600	0.0	70.4	18.1	10.4	55.5	36.0	7.7	2.5	68.1	31.9	2.9	1.5	91.0	0.55	0.47	0.05
40*	3600	0.0	72.0	18.1	10.3	51.8	33.0	8.8	6.6	68.0	28.7	2.7	2.0	97.0	0.34	0.24	0.20
41	3000	0.0	70.0	16.7	10.5	51.0	32.1	8.5	6.9	68.9	27.2	4.3	1.2	95.0	0.25	0.21	0.62
27	1600	0.1	66.1	17.5	9.4	50.3	39.8	5.0	3.1	62.4	30.1	3.1	1.4	98.5	0.32	0.13	0.05
43	1000	0.0	70.6	18.1	10.3	48.0	31.5	9.2	6.6	60.2	31.3	4.4	1.7	91.7	0.91	0.10	0.22

*Repeated measurements on the same specimen.

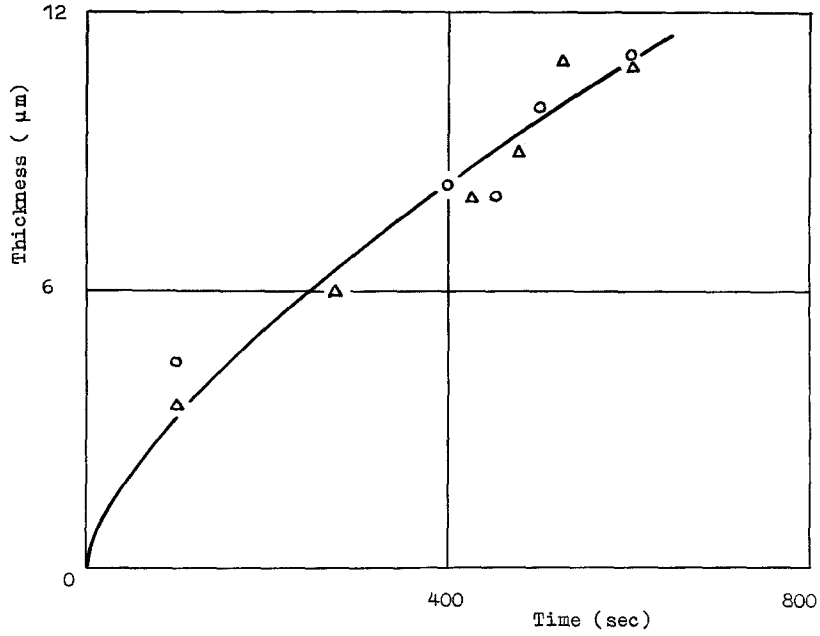

Figure 14 A plot of layer thickness against dipping time for an undersaturated melt. Temperature = 700° C; rotational speed, ω = 24.0 rad sec^{-1}. (○) High-purity aluminium melts; (△) commercial aluminium melts.

One suitable technique to produce stainless steel-to-aluminium transition joints is by means of interaction of a solid steel material with liquid aluminium under well-controlled temperature, time and hydrodynamic conditions with subsequent joint cooling until full solidification of the aluminium melt. A few transition pieces thus obtained are shown in Fig. 15.

Tensile tests of the butt-joined bimetallic pipes (25 to 30 mm diameter with a wall thickness of 1 to 2 mm and 65 to 80 mm total length) were performed at room temperature with a speed of 0.2 mm sec^{-1} [33]. A steel-to-aluminium pipe after the tensile test is shown in Fig. 16. The rupture of an aluminium part of the bimetallic pipes usually occurred at a distance 5 to 15 mm away from the junction. The breaking stress was 45 to 54 MPa, if the high-purity aluminium had been used as a starting material to make the transition joints. In the case of commercially pure aluminium, these values were somewhat greater: 74 to 95 MPa. The above values are usual for both melt materials [32].

The plastic properties of the aluminium part of the bimetallic pipes were also similar to those of the starting melt materials. This is due to a small level of contamination of the melts by the steel constituents during making the transition pieces. Thus, the tensile properties of the stainless steel-to-aluminium transition joints and those of the starting melt materials appear to be the same.

No change in tensile properties of the transition joints was revealed after the following thermal cycling treatments (100 cycles):

1. Cooling from 100 to −196° C in liquid nitrogen at a mean rate of 2° C sec^{-1}. Heating from −196 to 100° C in boiling water at a mean rate of 5° C sec^{-1}.
2. Cooling from 400 to −196° C in liquid nitrogen at a mean rate of 3° C sec^{-1}. Heating from −196 to 400° C in an electric resistance furnace in air at a mean rate of 3° C sec^{-1}.

Vacuum tests showed the transition pieces to be air-tight both initially and after thermal cycling.

4. Conclusions

The dissolution of an 18Cr–10Ni stainless steel in liquid aluminium was found by the rotating disc technique to be non-selective at 700 to 850° C. That is, during dissolution, all the elements pass from the steel into the aluminium melt in those ratios in which they are present in the steel bulk. The steel thus behaves like a single element.

The saturation concentration of iron from the steel

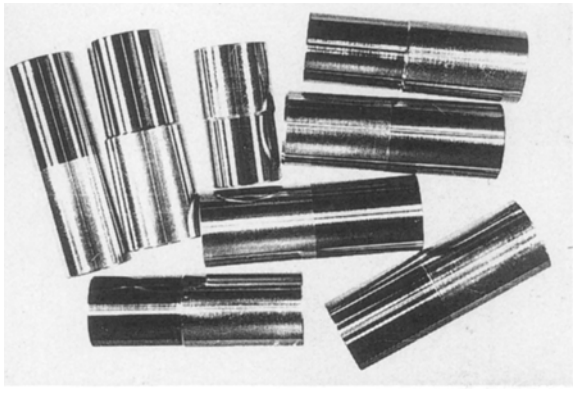

Figure 15 Steel-to-aluminium transition joints.

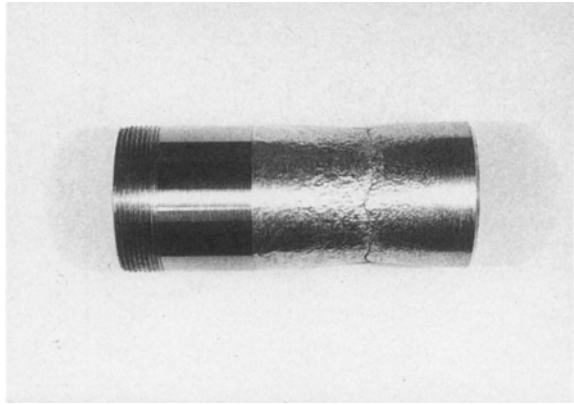

Figure 16 A stainless steel-to-aluminium bimetallic pipe after the tensile test. Starting melt material: commercially pure aluminium.

TABLE X Data of electron probe microanalysis of contents for an undersaturated melt

Specimen no.	Initial melt material	Dipping time (sec)	Layer thickness (μm)	Steel base				Intermetallic layer					Aluminium matrix			
				Al (%)	Fe (%)	Cr (%)	Ni (%)	Al (%)	Fe (%)	Cr (%)	Ni (%)	Al + Fe + Cr + Ni (%)	Al (%)	Fe (%)	Cr (%)	Ni (%)
16	High-purity aluminium	400	8	0.0	69.3	17.9	10.2	55.8	28.4	6.0	2.4	92.6	98.1	0.78	0.95	0.27
31	Commercial aluminium	475	9	0.0	70.5	19.1	9.8	55.9	22.3	5.2	1.4	84.8	96.2	0.15	0.17	0.07
4	High-purity aluminium	600	11	0.0	69.8	18.3	9.7	55.3	24.1	6.3	1.9	84.8	97.3	0.26	0.30	0.04

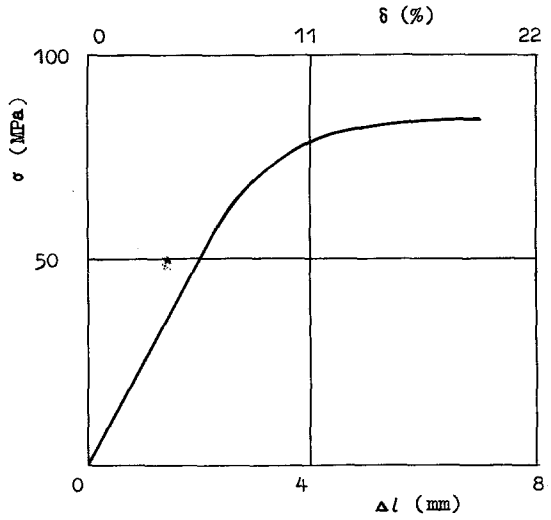

Figure 17 A plot of stress against elongation (absolute and relative) for the specimen shown in Fig. 16. Breaking stress = 80 MPa; total elongation = 19%.

into liquid aluminium and its solubility in the Al–Fe binary system at 700 and 750° C are the same, whereas at 800 and 850° C the former value is somewhat less than the latter one. The saturation concentration of chromium from the steel into liquid aluminium is less, and that of nickel is far less than their solubility values in the Al–Cr and Al–Ni binary systems, respectively.

No noticeable differences were revealed in values of the dissolution rate constant of the steel in different melts (melt materials: high-purity aluminium, commercially pure aluminium and an aluminium alloy containing 1% Fe and corresponding amounts of other elements from the steel investigated).

At a constant temperature, a linear dependence was observed between k and $\omega^{1/2}$ indicative of a diffusion-controlled character of the steel dissolution in liquid aluminium. The diffusion coefficient of iron from the steel across the diffusion boundary layer at the steel–aluminium interface in the bulk liquid aluminium was estimated to be $2.1 \times 10^{-9}\,m^2\,sec^{-1}$ at 700° C. This value is greater than the diffusion coefficient, $D_{Fe} = 1.24 \times 10^{-9}\,m^2\,sec^{-1}$, of iron from pure iron in liquid aluminium under similar conditions [6]. It should be noted that the latter value is in reasonable agreement with the findings of other authors. The following values are reported in the literature (at 700° C): $D_{Fe} = 1.40 \times 10^{-9}\,m^2\,sec^{-1}$ [34], $D_{Fe} = 1.24 \times 10^{-9}\,m^2\,sec^{-1}$ [35] (see also [1]) and $D_{Fe} = (1.27 \text{ to } 1.44) \times 10^{-9}\,m^2\,sec^{-1}$ [36].

Note that the value $D = 2.1 \times 10^{-9}\,m^2\,sec^{-1}$ is the diffusion coefficient not only for iron, but also for both chromium and nickel from the steel into liquid aluminium. These elements are not free to move independently across the diffusion boundary layer at the steel–aluminium interface. Instead, there is considerable mutual influence on their diffusion rates. The value $D = 2.1 \times 10^{-9}\,m^2\,sec^{-1}$ is clearly a compromise one, because at 700° C in appropriate binary systems $D_{Fe} = 1.24 \times 10^{-9}\,m^2\,sec^{-1}$ [6], $D_{Cr} = 1.97 \times 10^{-9}\,m^2\,sec^{-1}$ [3] and $D_{Ni} = 2.70 \times 10^{-9}\,m^2\,sec^{-1}$ [3]. (Roy and Chhabra [34] reported the experimental value $D_{Ni} = 3.86 \times 10^{-9}\,m^2\,sec^{-1}$ at 980 K.)

The temperature dependence of the dissolution rate constant of iron from steel into liquid aluminium does not obey the Arrhenius law. Moreover, the values of the dissolution rate constant were found to be the same at both 800 and 850° C. This is probably due, firstly, to a mutual influence of the elements on their diffusion rates across the diffusion boundary layer and, secondly, to a great change in melt viscosity with increasing content of alloying elements in the aluminium melt.

At 700° C, two intermetallic layers were found to form between the steel and the aluminium melt previously saturated with respect to the steel constituents. The compact layer adjacent to the steel surface was probably a solid solution based upon the Fe_2Al_5 compound. The crystallites of a solid solution on the basis of the $FeAl_3$ compound formed the framework of the layer adjacent to the melt material. The pores of this framework were filled by aluminium. The growth kinetics of the layers were found to be "paralinear". The thickness of the layer adjacent to the steel surface tends with increasing dipping time to a limiting value of 10 μm while the growth of the layer adjacent to the melt material after a certain period of non-linear growth becomes linear.

In the case of undersaturated aluminium melts, only one intermetallic layer, 3 to 11 μm thick, was found to form between the steel and the melt material (high-purity aluminium or commercially pure aluminium) at 700° C for 100 to 600 sec. Its exact composition could not be established by any available technique, including electron probe microanalysis.

The stainless steel-to-aluminium transition joints with good mechanical properties (at least not worse than those of commercially pure aluminium) can be obtained by means of interaction of a solid steel material with liquid aluminium under well-controlled conditions with subsequent joint cooling until the solidification of the melt material.

References

1. V. N. YEREMENKO, Ya. V. NATANZON and V. P. TITOV, *Fiz. Khim. Mech. Mater.* **6** (1978) 3.
2. V. N. YEREMENKO, Ya. V. NATANZON and V. I. DYBKOV, *ibid.* **6** (1984) 3.
3. A. P. GULYAEV, "Metallovedeniye" (Metallurgiya, Moscow, 1978) p. 483 (in Russian).
4. N. KOMATSU, M. NAKAMURA and H. FUJITA, *J. Inst. Light Metals* **18** (1968) 474.
5. V. N. YEREMENKO, Ya. V. NATANZON and V. I. DYBKOV, *J. Less-Common Metals* **50** (1976) 29.
6. *Idem, J. Mater. Sci.* **16** (1981) 1748.
7. V. I. DYBKOV, *Poroshkovaya Metallurgiya* **3** (1980) 54.
8. A. G. WARD and J. W. TAYLOR, *J. Inst. Metals* **86** (1957) 36.
9. S. MINOWA, M. KOSAKA, M. KATO and M. MIZUTA, *J. Iron Steel Inst. Jpn* **49** (1963) 1596 (in Japanese).
10. S. MINOWA, M. KOSAKA and M. MIZUTA, *ibid.* **50** (1964) 644 (in Japanese).
11. G. EGGELER, W. AUER and H. KAESCHE, *J. Mater. Sci.* **21** (1986) 3348.
12. T. N. NAZARCHUK, G. T. KABANNIK and V. I. DYBKOV, *Fiz. Khim. Mech. Mater.* **5** (1985) 19.
13. Ya. V. NATANZON and V. I. DYBKOV, *ibid.* **6** (1987) 97.
14. A. E. VOL, "Structura i Svoystva Binarnikh Metallicheskikh System", Vol. 1 (Fizmatgiz, Moscow, 1959) pp. 222, 407.

15. V. N. YEREMENKO (ed.) "Fizicheskaya Khimiya Neoganicheskikh Materialov", Vol. 2 (Naukova Dumka, Kiev, 1988) p. 66.
16. V. I. DYBKOV, *Zh. Fiz. Khimii* **53** (1979) 2868.
17. V. G. LEVICH, "Fiziko-Khimicheskaya Hydrodynamika" (Fizmatgiz, Moscow, 1959) p. 77 (in Russian).
18. T. F. KASSNER, *J. Electrochem. Soc.* **114** (1967) 689.
19. Ya. V. NATANZON, S. A. SUKHOREBRAYA and V. I. DYBKOV, *Fiz. Khim. Mech. Mater.* **2** (1986) 112.
20. E. S. LEVIN, *Izv. Akad. Nauk SSSR Met.* **5** (1971) 72.
21. M. NIINOMI, Y. UEDA and M. SANO, *Trans. Jpn. Inst. Metals* **23** (1982) 780.
22. V. I. DYBKOV, IPM Technical Report No. 81030999 (1985).
23. M. HANSEN and K. ANDERKO, (eds.) "Constitution of Binary Alloys", Vol. 1 (Gostekhizdat, Moscow, 1962) p. 106 (Russian translation).
24. M. NIINOMI and Y. UEDA, *Trans. Jpn. Inst. Metals* **11** (1982) 709.
25. V. I. DYBKOV, *Poroshkovaya Metallurgiya* **12** (1986) 44.
26. L. I. MIRKIN, "Spravochnik po Rentgenostrukturnomu Analizu Polikristallov" (Fizmatgiz, Moscow, 1961) p. 458 (in Russian).
27. P. KOFSTAD, "High Temperature Oxidation of Metals" (Wiley, New York, 1968) Ch. 7 (Russian translation).
28. V. I. DYBKOV, *J. Mater. Sci.* **21** (1986) 3085.
29. T. HEUMANN and S. DITTRICH, *Z. Metallkde.* **50** (1959) 617.
30. V. I. DYBKOV, *J. Mater. Sci.* **21** (1986) 3078.
31. R. R. IRVING, *Iron Age* **196** (1965) 97.
32. V. R. RYABOV, "Svarka Plavleniyem Aluminiya so Stal'u (Naukova Dumka, Kiev, 1969) Chs. 1 to 3, 5 (in Russian).
33. Ya. V. NATANZON, M. L. GORB and V. I. DYBKOV, *Fiz. Khim. Mech. Mater.* **3** (1980) 51.
34. A. K. ROY and R. P. CHHABRA, *Metall. Trans.* **19A** (1988) 273.
35. G. I. BARINOV, *Technol. Mater. Electr. Tekhn.* **2** (1970) 82.
36. K. UEMURA, *J. Iron Steel Inst. Jpn* **25** (1939) 24 (in Japanese).

Received 6 April
and accepted 28 September 1989